Layered $Li_xNi_yMn_yCo_{1-2y}O_2$ Cathodes for Lithium Ion Batteries: Understanding Local Structure via Magnetic Properties

Natasha A. Chernova,*,† Miaomiao Ma,† Jie Xiao,† M. Stanley Whittingham,† Julien Breger,‡ and Clare P. Grey‡

Institute for Materials Research, State University of New York at Binghamton, Binghamton, New York 13902-6000, and Department of Chemistry, State University of New York at Stony Brook, Stony Brook, New York 11794

Received March 30, 2007. Revised Manuscript Received July 11, 2007

The magnetic properties of layered $LiNi_yMn_yCo_{1-2y}O_2$ ($y = 0.5$, 0.45, 0.4, and $^1/_3$) compounds are studied in order to understand the transition metal ion distributions via their magnetic interactions. In $LiNi_{0.5}Mn_{0.5}O_2$, an increase of magnetization is found below 100 K with ac magnetic susceptibility revealing broad peaks at 96, 40, 13, and 7 K. The low-temperature neutron diffraction and heat capacity studies do not reveal long-range magnetic ordering; the magnetic component of heat capacity shows a broad peak at 10 K. This behavior is explained by assuming a nonrandom distribution of transition metals. The 96 K transition is attributed to the ordering of clusters of Ni^{2+} spins in the transition metal and lithium layers, which are coupled by a 180° superexchange mechanism. The wide 40 K peak is explained by an increase of the cluster size due to intralayer Ni and Mn spin ordering, by analogy with antiferromagnetic ordering transitions in Li_2MnO_3 at 36.5 K and in $NaNi_{0.5}Mn_{0.5}O_2$ at 55 K. The continuing increase of net magnetization in this temperature range indicates at least partial ferromagnetic interlayer ordering in $LiNi_{0.5}Mn_{0.5}O_2$ as opposed to Li_2MnO_3 and $NaNi_{0.5}Mn_{0.5}O_2$, which is caused by Ni^{2+} ions in the lithium layer. The 7−13 K anomalies are ascribed to the freezing of cluster magnetic moments. With increasing Co content, the amount of Ni^{2+} in the transition metal layer decreases, the cluster ordering transitions disappear, and only the spin-glass freezing is observed in $LiNi_{0.4}Mn_{0.4}Co_{0.2}O_2$ and $LiNi_{1/3}Mn_{1/3}Co_{1/3}O_2$ at 10 and 7 K, respectively. This is consistent with the lack of long-range ordering of the transition metal ions in these compounds. The evolution of the magnetic properties upon electrochemical cycling of $LiNi_{0.5}Mn_{0.5}O_2$ is studied. Oxidation of Ni^{2+} ($S = 2$) to Ni^{3+} ($S = ^1/_2$) to Ni^{4+} ($S = 0$) is observed upon lithium removal as well as breakage of the partial magnetic ordering when 0.3 Li is removed. The latter is explained by the preferential oxidation of the Ni ions in the transition metal layers involved in the 180° magnetic exchange.

Introduction

Layered $LiNi_{1-y-z}Mn_yCo_zO_2$ oxides have attracted much attention as cathode materials for lithium ion batteries.[1−6] These materials are good candidates to replace $LiCoO_2$ used in the original commercially available lithium ion battery introduced by SONY.[7−9] $LiCoO_2$ shows stable electrochemical performance over hundreds of cycles, but it delivers only half of the theoretically possible capacity; in addition, this material is expensive and not environmentally friendly.[2,7] A promising way to modify this material is to substitute Co with Mn and Ni in equal amounts, making $LiNi_yMn_yCo_{1-2y}O_2$.[10−14] These compounds have the layered O3 structure, space group $R\bar{3}m$ (Figure 1) and the oxidation states of Ni and Mn are 2+ and 4+, respectively, as shown from first-principle calculations, X-ray absorption, and magnetic studies.[15−18] Thus, Ni^{2+} is the electrochemically active ion, while the octahedrally coordinated Mn^{4+} ion, with its d^3 electronic configuration, helps to ensure the stability of the structure. However, the close similarity of the ionic radii of

* Corresponding author. Phone: +1-607-777-4298. Fax: +1-607-777-4623. E-mail: nchernova@gmail.com.
† State University of New York at Binghamton.
‡ State University of New York at Stony Brook.

(1) Ohzuku, T.; Ariyoshi, M.; Makimura, Y.; Yabuuchi, N.; Sawai, K. *Electrochemistry* **2005**, *73*, 2.
(2) Whittingham, M. S. *Chem. Rev.* **2004**, *104*, 4271.
(3) Liu, Z.; Yu, A.; Lee, J. Y. *J. Power Sources* **1999**, *81-82*, 416.
(4) Yoshio, M.; Noguchi, H.; Itoh, J.; Okada, M.; Mouri, T. *J. Power Sources* **2000**, *90*, 176.
(5) Spahr, M. E.; Novak, P.; Schnyder, B.; Haas, O.; Nesper, R. *J. Electrochem. Soc.* **1998**, *145*, 1113.
(6) Kobayashi, H.; Sakaebe, H.; Kageyama, H.; Tatsumi, K.; Arachi, Y.; Kamiyama, T. *J. Mater. Chem.* **2003**, *13*, 590.
(7) Mitzushima, K.; Jones, P. C.; Wiseman, P. J.; Goodenough, J. B. *Mater. Res. Bull.* **1980**, *15*, 783.
(8) Goodenough, J. B.; Mizuchima, K. U.S. Patent 4,302,518, 1981.
(9) Nishi, Y. In *Lithium Ion Batteries*; Wakihara, M., Yamamoto, O., Eds.; Kodansha: Tokyo, 1998; p 181.
(10) Sun, Y.; Ouyang, C.; Wang, Z.; Huang, X.; Chen, L. *J. Electrochem. Soc.* **2004**, *151*, A504.
(11) Kim, J.-M.; Chung, H.-T. *Electrochim. Acta* **2004**, *49*, 937.
(12) MacNeil, D. D.; Lu, Z.; Dahn, J. R. *J. Electrochem. Soc.* **2002**, *149*, A1332.
(13) Lu, Z.; MacNeil, D. D.; Dahn, J. R. *Electrochem. Solid State Lett.* **2001**, *4*, A191.
(14) Jiang, J.; Buhrmester, T.; Eberman, K. W.; Krause, L. J.; Dahn, J. R. *J. Electrochem. Soc.* **2005**, *152*, A19.
(15) Reed, J.; Ceder, G. *Electrochem. Solid State Lett.* **2002**, *5*, A145.
(16) Arachi, Y.; Kobayashi, H.; Emura, S.; Nakata, Y.; Tanaka, M.; Asai, T. *Chem. Lett.* **2003**, *32*, 60.
(17) Ngala, J. K.; Chernova, N. A.; Ma, M.; Mamak, M.; Zavalij, P. Y.; Whittingham, M. S. *J. Mater. Chem.* **2004**, *14*, 214.
(18) Deb, A.; Bergmann, U.; Cramer, S. P.; Cairns, E. J. *J. Appl. Phys.* **2005**, *97*, 113523.

10.1021/cm0708867 CCC: $37.00
Published on Web 08/23/2007

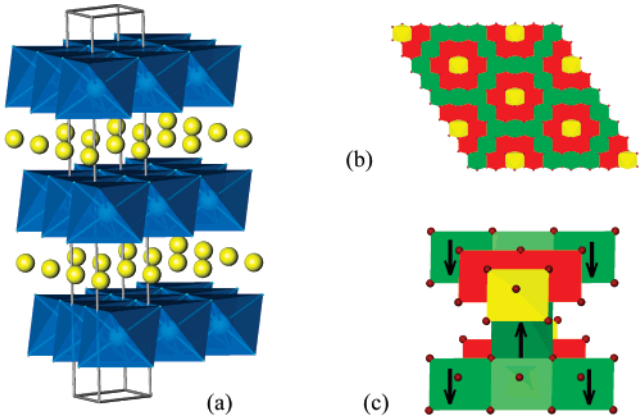

Figure 1. (a) Structure of $LiNi_xMn_xCo_{1-2x}O_2$: metal layer shown in blue and lithium ions are yellow. (b) Flower order of the transition metals proposed for $LiNi_{0.5}Mn_{0.5}O_2$: LiO_6 octahedra, yellow; MnO_6, red; NiO_6, green. (c) The 180° antiferromagnetic (AF) exchange between Ni^{2+} ions in the flower structure. The NiO_6 octahedron in the lithium layer is dark-green. Spins in the "corner" (bright-green) NiO_6 octahedra are fixed by 180° AF coupling to interlayer Ni^{2+}; the alignment of the spins in the "middle" NiO_6 octahedra (pale green) is not known.

Ni^{2+} and Li^+ leads to significant mixing of these ions, which may hamper lithium diffusion and reduce the electrochemical performance. Despite this, $LiNi_{0.5}Mn_{0.5}O_2$ with 8% Li/Ni mixing shows surprisingly good electrochemical properties, at least at low rates.[5,19,20] Extensive structural studies of both pristine and lithium-deintercalated $LiNi_{0.5}Mn_{0.5}O_2$ have been performed to understand the mechanism of lithium removal and insertion in this compound.[21−25] Electron diffraction, NMR, and pair-distribution function analysis of the X-ray and neutron diffraction have shown a strong ordering tendency between the transition metal (TM) and lithium ions. First-principle calculations have identified a low-energy structure, termed the "flower structure", in which $^1/_{12}$ of the Ni^{2+} ions are located in the lithium layer and the same amount of Li is in the transition metal layer. The Li ions in the transition metal layers are surrounded by 6 Mn^{4+} ions ($LiMn_6$ clusters), and these are surrounded by 12 Ni^{2+} ions (Figure 1).[26] The experimental data provide evidence for this type of ordering but indicate that this ordering is far from perfect.[24]

Magnetic interactions play an important role in increasing the stability of the flower structure. The interslab Ni^{2+} magnetic moments are coupled by strong 180° antiferromagnetic (AF) exchange to the magnetic moments of the Ni^{2+} in the transition metal layer, lowering the total electronic energy of the flower structure (Figure 1). The formation of magnetic clusters around the interslab Ni^{2+} ions is not new and is known to strongly affect the magnetic properties of layered compounds. For example, a number of controversial magnetic properties were ascribed to $LiNiO_2$ (see, for example, ref 27 and references therein) before its nonstoichiometric and disordered nature, expressed as $[Li_{1-x}Ni_x^{2+}]_{3a}[Ni_x^{2+}Ni_{1-x}^{3+}]_{3b}O_2$, was appreciated and accounted for in the analysis of the magnetic data.[27−29] Even now the nature of the $LiNiO_2$ ground state remains unclear; the latest findings indicating the important role of orbital coupling.[30,31] This shows how complicated the magnetism of layered compounds with structural disorder can be.

The amount of Ni^{2+} in the lithium layer of $LiNi_yMn_yCo_{1-2y}O_2$ can be reduced by increasing the Co content.[17] In this work, we reveal the evolution of the magnetic properties of $LiNi_yMn_yCo_{1-2y}O_2$ with increasing Co content from $LiNi_{0.5}Mn_{0.5}O_2$ to $LiNi_{1/3}Mn_{1/3}Co_{1/3}O_2$. On the basis of the observed magnetic transitions, we comment on the degree of order in the flower structure and discuss the possibility of ordering in $LiNi_{1/3}Mn_{1/3}Co_{1/3}O_2$. We also study the magnetic properties of $Li_xNi_{0.5}Mn_{0.5}O_2$ upon cycling of lithium to understand whether and how the TM ions are affected by this process. The results are compared with those from recent magnetism, EPR, and theoretical studies of $Li_xMn_{0.5}Ni_{0.5}O_2$.[32−35]

Experimental Section

$LiNi_yMn_yCo_{1-2y}O_2$ compounds with $y = 0.5$ (further called compound 550), 0.45 (compound 992), 0.4 (compound 442), and $^1/_3$ (compound 333) were synthesized by mixed hydroxide method followed by high-temperature solid-state reaction. The labeling scheme for the four compounds indicates the Ni:Mn:Co ratio; for example, 992 contains 0.45 Ni, 0.45 Mn, and 0.1 Co ions per formula unit. The details of the synthesis and characterization may be found elsewhere.[36] The compounds were characterized by X-ray diffraction on a Scintag XDS2000 $\theta-\theta$ powder diffractometer equipped with a Ge(Li) solid-state detector and Cu Kα sealed tube ($\lambda = 1.541\,78$ Å). Data were collected over the range of 15−90° 2θ with a step size of 0.02° step and exposure of 5 s for routine characterization and over the range of 15−120° 2θ with a step size of 0.02° step and exposure of 10 s for the structure refinement. The Rietveld refinement was conducted using the GSAS/EXPGUI package.[37,38] The details of preparation and characterization of Li_x-

(19) Ohzuku, T.; Makimura, Y. *Chem. Lett.* **2001**, *8*, 744.
(20) Kang, K. S.; Meng, Y. S.; Breger, J.; Grey, C. P.; Ceder, G. *Science* **2006**, *311*, 977.
(21) Meng, Y. S.; Ceder, G.; Grey, C. P.; Yoon, W.-S.; Shao-Horn, Y. *Electrochem. Solid State Lett.* **2004**, *7*, A155.
(22) Yoon, W.-S.; Iannopollo, S.; Grey, C. P.; Carlier, D.; Gorman, J.; Reed, J.; Ceder, G. *Electrochem. Solid State Lett.* **2004**, *7*, A167.
(23) Breger, J.; Jiang, M.; Dupre, N.; Meng, Y. S.; Shao-Horn, Y.; Ceder, G.; Grey, C. P. *J. Solid State Chem.* **2005**, *178*, 2575.
(24) Breger, J.; Dupre, N.; Chupas, P. J.; Lee, P. T.; Proffen, T.; Parise, J. B.; Grey, C. P. *J. Am. Chem. Soc.* **2005**, *127*, 7529.
(25) Miao, S.; Kocher, M.; Rez, P.; Fultz, B.; Ozawa, Y.; Yazami, R.; Ahn, C. C. *J. Phys. Chem. B* **2005**, *109*, 23473.
(26) Van der Ven, A.; Ceder, G. *Electrochem. Commun.* **2004**, *6*, 1045.
(27) Reimers, J. N.; Dahn, J. R.; Greedan, J. E.; Stager, C. V.; Liu, G.; Davidson, I.; von Sacken, U. *J. Solid State Chem.* **1993**, *102*, 542.
(28) Chappel, E.; Nunez-Regueiro, M. D.; Chouteau, G.; Sulpice, A.; Delmas, C. *Solid State Commun.* **2001**, *119*, 83.
(29) Chappel, E.; Nunez-Regueiro, M. D.; de Brion, S.; Chouteau, G.; Bianchi, V.; Caurant, D.; Baffier, N. *Phys. Rev. B.* **2002**, *66*, 132412.
(30) Reynaud, F.; Mertz, D.; Celestini, F.; Debierre, J.-M.; Ghorayeb, A. M.; Simon, P.; Stepanov, A.; Voiron, J.; Delmas, C. *Phys. Rev. Lett.* **2001**, *86*, 3638.
(31) Chung, J.-H.; Proffen, Th.; Shamoto, S.; Ghorayeb, A. M.; Croguennec, L.; Tian, W.; Sales, B. C.; Jin, R.; Mandrus, D.; Egami, T. *Phys. Rev. B* **2005**, *71*, 064410.
(32) Stoyanova, R.; Zhecheva, E.; Alcantara, R.; Tirado, J. L. *J. Mater. Chem.* **2006**, *16*, 359.
(33) Stoyanova, R.; Zhecheva, E.; Vassilev, S. *J. Solid State Chem.* **2006**, *179*, 378.
(34) Abdel-Ghany, A.; Zaghib, K.; Gendron, F.; Mauger, A.; Julien, C. M. *Electrochim. Acta* **2007**, *52*, 4092.
(35) Hinuma, Y.; Meng, Y. S.; Kang, K.; and Ceder, G. *Chem. Mater.* **2007**, *19*, 1790.
(36) Ma, M.; Chernova, N. A.; Toby, B. H.; Zavalij, P. Y.; Whittingham, M. S. *J. Power Sources* **2007**, *165*, 517.
(37) Toby, B. H. *J. Appl. Crystallogr.* **2001**, *34*, 210.
(38) Larson, A. C.; Von Dreele, R. B. *Los Alamos National Laboratory Report LAUR* **2000**, *86*, 748.

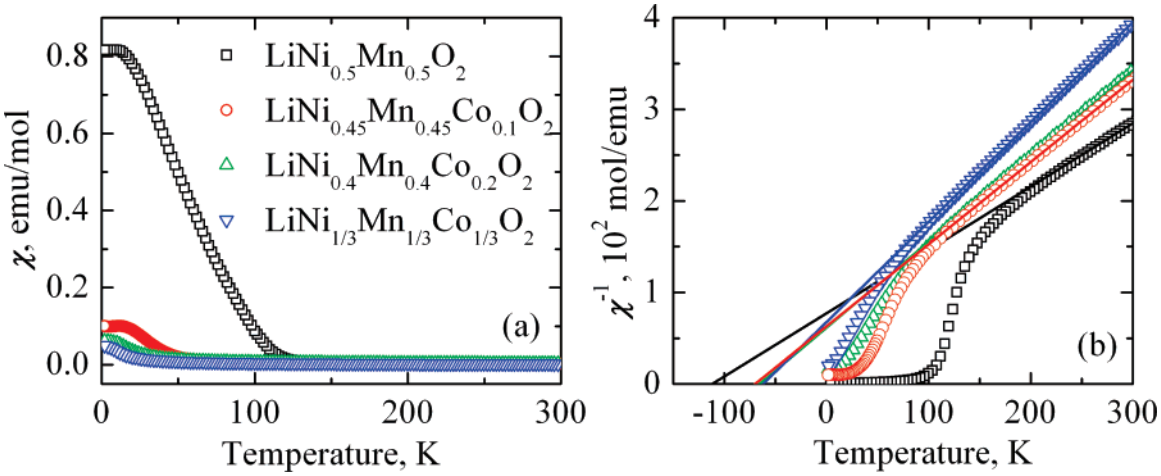

Figure 2. (a) Temperature dependences of magnetic susceptibilities of $LiNi_yMn_yCo_{1-2y}O_2$ and (b) the reciprocal susceptibilities and their fit to the Curie−Weiss law (solid lines).

$Ni_{0.5}Mn_{0.5}O_2$ materials may be found in ref 39. Two sets of samples $Li_xNi_{0.5}Mn_{0.5}O_2$ were studied, one being cycled in large cells with graphite only and the other charged in small cells with both graphite and binder. The first set of samples (with $x = 0.6$, 0.4, and 0.06) was prepared for investigation by neutron diffraction, and the electrochemical curves for the samples have been presented elsewhere.[39] These were cycled at a very slow rate (C/200), due to the large mass of active cathode in the cells (300 mg). The second set of samples was prepared (in smaller cells) to investigate samples with higher Li contents; samples were also prepared with the same nominal Li contents to examine differences between the two sets of samples. The smaller cells were cycled with a rate of C/20 in coin cells (CR2032, Hohsen Corp.; 15 mg of active cathode material). Lithium contents were calculated from the electrochemical curves by assuming 100% Coulombic efficiency.

The magnetic properties were studied with a Quantum Design SQUID magnetometer (MPMS XL-5). The temperature dependences of the dc magnetization were measured on cooling the samples from either 400 or 298 to 2 K in a magnetic field of 1000 Oe. Field-cooled (FC) and zero-field-cooled (ZFC) magnetizations were measured from 298 to 2 K in magnetic fields of either 10 or 100 Oe. FC susceptibility was measured by cooling the sample in the magnetic field; before taking ZFC data, the remanent magnetic field was quenched to less than 3 mOe, the sample was cooled to 2 K, the magnetic field was applied, and the temperature dependence was measured while the sample was heated. The magnetization curves were measured at 5 K in the magnetic field up to 5 T; the samples were zero-field cooled before these experiments. The temperature dependences of the ac susceptibility were measured in the ac field $H = 4$ Oe at various frequencies f from 0.05 to 1000 Hz. The sample was zero-field cooled as described above and the ac data were collected while the sample was heated. For the electrochemically cycled materials containing graphite and Teflon binding, the temperature dependence of magnetization of the graphite and Teflon was measured separately and subtracted from the data. The temperature dependence of the heat capacity was measured using a Quantum Design PPMS system in temperature range from 300 to 2 K. The details of low-temperature neutron diffraction experiments are presented in the Supporting Information.

Results

The temperature dependences of the dc magnetic susceptibility $\chi = M/H$, where M is magnetization and H is the applied magnetic field, are presented in Figure 2a together with their reciprocals (Figure 2b). At high temperatures, these dependences follow the Curie−Weiss law $\chi = C/(T - \Theta)$, where C is the Curie constant and Θ is the Curie−Weiss temperature. At low temperatures, an increase of the magnetic susceptibility is observed, being the most pronounced in the 550 compound; with increasing Co content it diminishes and shifts to lower temperatures. The high-temperature parts of the $\chi^{-1}(T)$ dependences (typically above 200 K) were fit to the Curie−Weiss law (solid lines in Figure 2b) and the parameters are summarized in Table 1. With increasing Co content the Curie constant, the absolute value of Θ, and the average magnetic moment per transition metal ion μ all decrease. The theoretical magnetic moments calculated by assuming Mn^{4+} ($S = {}^3/_2$, $g = 2$) and Ni^{2+} ($S = 1$, $g = 2$) oxidation states agree reasonably well with the experimental ones. The negative Θ values indicate the predominance of antiferromagnetic exchange interactions in these compounds.

Table 1. Magnetic Parameters of the $LiNi_yMn_yCo_{1-2y}O_2$ Compounds

sample name	C, emu K/mol	Θ, K	μ_{exp}, μ_B	μ_{theor}, μ_B	M_r, emu/mol	H_c, Oe	T_b, K
55	1.446(4)	−111.8(6)	3.40(1)	3.39	710.0	1316(2)	120
992	1.227(2)	−87.9(3)	3.13(1)	3.22	35.8	456(1)	60
442	1.068(2)	−65.8(2)	2.92	3.03	4.9	83(1)	11
333	0.916(1)	−62.1(1)	2.71	2.77	0.5	11(1)	7

[a] Theoretical magnetic moments are calculated by assuming Ni^{2+} ($S = 1$) and Mn^{4+} ($S = {}^3/_2$) oxidation states.

The strong increase of the susceptibility observed in the 550 compound may indicate magnetic ordering with net magnetic moment formation. As opposed to the very sharp magnetic ordering transitions that occur in ferro- or ferrimagnets, the transition in the 550 compound is smeared over a wide temperature range. This is typical of magnetic ordering within finite size clusters, which may or may not lead to long-range order at lower temperatures. With increasing concentration of the nonmagnetic Co^{3+} ions (low-spin d^6 configuration), the number and size of magnetic clusters decreases, leading to a decrease of the total magnetic moment per formula unit.

The magnetization curves reveal a large hysteresis loop in the 550 compound, while in the Co-containing compounds

(39) Breger, J.; Meng, Y. S.; Hinuma, Y.; Kumar, S.; Kang, K.; Shao-Horn, Y.; Ceder, G.; Grey, C. P. *Chem. Mater.* **2006**, *18*, 4768.

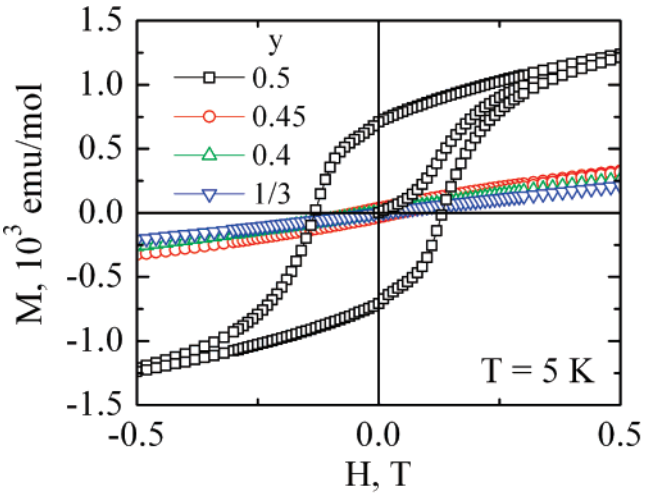

Figure 3. The magnetization curves of the $LiNi_yMn_yCo_{1-2y}O_2$ compounds.

the hysteresis is much less pronounced, becoming negligible in the 333 compound (Figure 3). The magnetizations do not reach saturation in a 5 T magnetic field, in agreement with the dominance of antiferromagnetic exchange. The parameters of the hysteresis loops such as the remanent magnetization M_r and the coercive field H_c are summarized in Table 1. Apparently, in the 550 compound the size of magnetically ordered clusters is large enough to result in large remanent magnetization and coercivity. In the Co-containing compounds, the cluster concentration and size both decrease, which results in a drop of the remanent magnetization and coercivity.

FC/ZFC data can be used to distinguish between magnetic ordering within large-size clusters and cluster-glass or spin-glass freezing (Figure 4). The 550 compound shows the largest difference between FC and ZFC curves and the highest blocking temperature of about 120 K, which is consistent with the ferro- or ferrimagnetic ordering within large clusters. The ZFC curve of the 550 compound shows two very broad maxima: one at about 95 K and the other at 13 K. In the 442 and 333 compounds, the blocking temperature is significantly lower, the difference between FC and ZFC curves is small, and the ZFC susceptibility shows a cusp at the blocking temperature similar to that observed in spin glasses. The 992 compound with 0.1 Co lies somewhere in between; its blocking temperature is still high, around 60 K, but the difference between FC and ZFC is not large; both FC and ZFC curves show a maximum centered at about 23 K.

The FC/ZFC curves of the 442 and 333 compounds are consistent with spin-glass transitions, in which collective freezing of individual ion magnetic moments occurs. In these compounds, the magnetic Ni^{2+} and Mn^{4+} ions are well-diluted with nonmagnetic Co^{3+} ions, and the requisite randomness required for spin glasses is generated this way. The other required component, magnetic frustration, may be provided by the geometry of the close-packed TM layer assuming antiferromagnetic exchange, as discussed later. In the 550 compound, the small magnetization observed under ZFC conditions may be explained by magnetic moments of different clusters freezing at random. The intermediate case of the 992 compound is also consistent with cluster-glass behavior; the difference between 550 and 992 compounds originates from smaller cluster size and concentration in the latter compound.

In order to confirm these hypotheses, we have studied the temperature dependences of the ac magnetic susceptibilities of the compounds at various frequencies. The representative results for the 550 and 442 compounds are summarized in Figures 5 and 6. In the 550 compound, both the real (χ') and imaginary (χ'') components of the ac susceptibility show frequency-dependent maxima around 96 K. The positions of these maxima do not change with frequency, thus pointing toward magnetic ordering rather than "glassy" transition. On the other hand, the observed maxima are wide, the frequency dependence is preserved below the transition temperature, and additional maxima are found at 40 and 7 K for $\chi''(T)$ and at 13 K for the $\chi'(T)$ dependences. These data indicate that the magnetic ordering occurs in the presence of some structural disorder and that the spin rearrangement continues down to 7 K.

In the case of the 442 compound, the maxima of $\chi'(T)$ and $\chi''(T)$ are observed around 10 K; in contrast to the 550 compound, there is a clear shift of these maxima toward lower temperatures when the ac frequency is decreased. The temperature shift per degree of frequency $\Delta T_f/[T_f\,\Delta(\log\,\omega)]$, where T_f is the freezing temperature and ω is the angular frequency, is about 0.01, the same as in many spin glasses.[40] We have calculated the temperature dependence of the spin relaxation time (τ) by assuming that the $\chi'(T)$ and $\chi''(T)$ peaks occur when $\omega\tau = 1$.[40] Figure 7 illustrates the $\tau(T)$ dependence obtained from the peak position of $\chi''(T)$ at various frequencies. The relaxation time decreases by 3 orders of magnitude when the spin-glass transition is approached from the high-temperature side. To analyze this dependence, we assume a conventional critical slowing down of spin fluctuations on approaching the spin-glass transition, in which case the $\tau(T)$ dependence can be described by $\tau = \tau_0(T/T_f - 1)^{-z\nu}$, where τ_0 is the characteristic relaxation time, z is the dynamical critical exponent, and ν is the critical exponent of the spin correlation length.[40] The best fit represented by the solid line in Figure 7 produces $\tau_0 \approx 10^{-13}$ s, $T_f = 9.6(1)$ K, and $z\nu = 8.5(9)$. The values of τ_0 and $z\nu$ agree very well with values typical of spin glasses. Similar features were found in the ac susceptibility data for the 333 compound, leading to the conclusion that a randomness in the TM distribution exists in our materials.

In order to check whether or not long-range magnetic ordering is established in the 550 compound, we studied the temperature dependence of the heat capacity and obtained low-temperature neutron diffraction data. The neutron diffraction data (see the Supporting Information) do not reveal any additional magnetic peaks below 100 K or a significant intensity change of the existing peaks, indicating absence of a long-range magnetic order. Consistent with this, the temperature dependence of the heat capacity presented in Figure 8 does not show the λ features that are expected for a magnetic ordering transition; however, a noticeable drop

(40) Mydosh, J. A. *Spin Glasses: An Experimental Introduction*; Taylor & Francis: London, 1993.

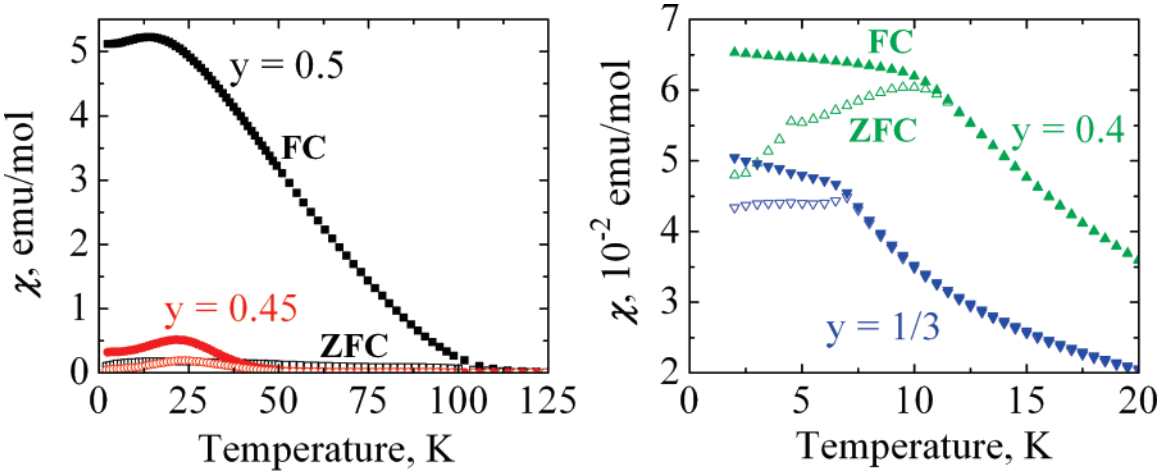

Figure 4. Field-cooled (solid symbols) and zero-field-cooled (open symbols) magnetic susceptibilities of $LiNi_yMn_yCo_{1-2y}O_2$ compounds measured in a magnetic field of 100 Oe ($y = 0.5$ and 0.4) and 10 Oe ($y = 0.45$ and $^1/_3$).

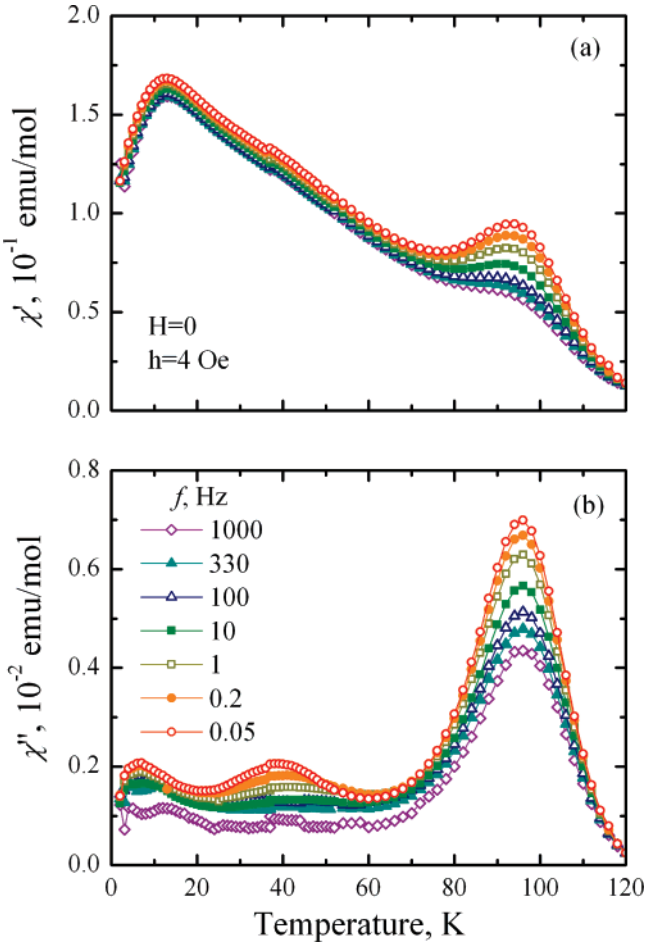

Figure 5. Temperature dependence of the real χ' (a) and imaginary χ'' (b) components of the ac susceptibility of $LiNi_{0.5}Mn_{0.5}O_2$ in an ac field of 4 Oe at various frequencies.

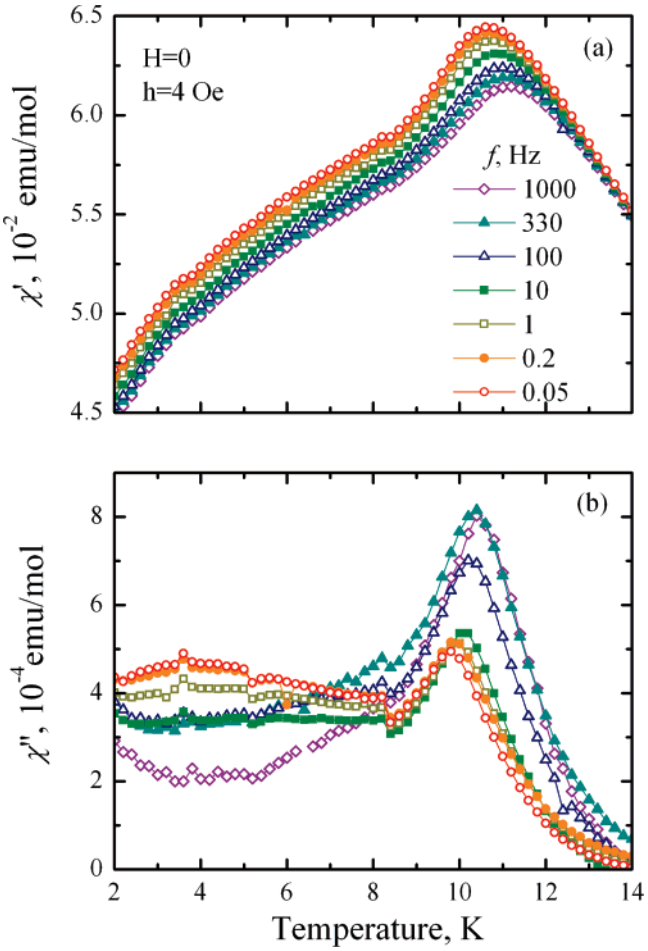

Figure 6. Temperature dependence of the real χ' (a) and imaginary χ'' (b) components of the ac susceptibility of $LiNi_{0.4}Mn_{0.4}Co_{0.2}O_2$ in an ac field of 4 Oe at various frequencies.

of heat capacity is found below 10 K. This data is compared with the heat capacity of isostructural compounds $Li_{0.99}Ni_{1.01}O_2$[41] and $LiCoO_2$[42] (Figure 8). The heat capacity of $LiCoO_2$ is significantly lower than that of the 550 compound, which cannot be explained simply by the absence of a magnetic contribution to the heat capacity in $LiCoO_2$.[42] The heat capacity of $Li_{0.99}Ni_{1.01}O_2$ is close to that of $LiNi_{0.5}Mn_{0.5}O_2$ in the temperature range 50−150 K. Below 20 K, the heat capacity of $Li_{0.99}Ni_{1.01}O_2$ shows an increase that may be associated with an onset of spin glass freezing observed in near stoichiometric $LiNiO_2$ at about 10 K.[29] Above 10 K, $Li_{0.99}Ni_{1.01}O_2$ is paramagnetic, so its heat capacity can be used as an estimate for the lattice component for the 550 compound, extrapolating the dependence to low tempera-

(41) Kawaji, H.; Oka, T.; Tojo, T.; Atake, T.; Hirano, A.; Kanno, R. *Solid State Ionics* **2002**, *152*−153, 195.
(42) Kawaji, H.; Takematsu, M.; Tojo, T.; Atake, T.; Hirano, A.; Kanno, R. *J. Therm. Anal. Calorim.* **2002**, *68*, 833.

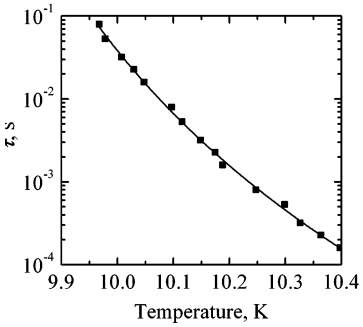

Figure 7. The temperature dependence of the characteristic spin relaxation time in $LiNi_{0.4}Mn_{0.4}Co_{0.2}O_2$ (solid squares) and its fit to the scaling law (solid line).

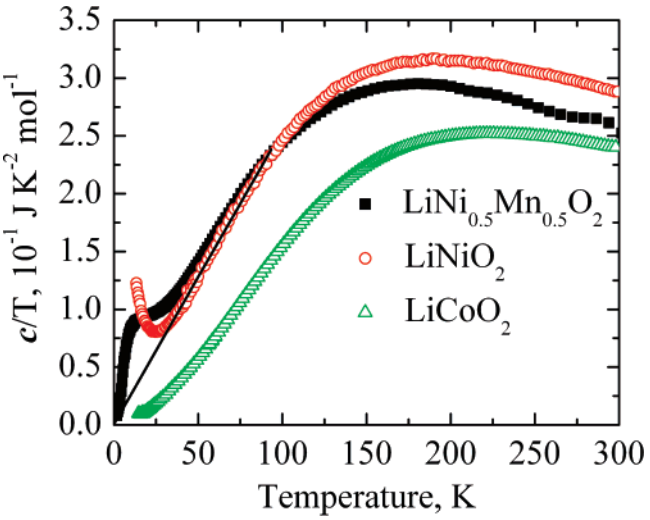

Figure 8. Temperature dependences of the specific heats of $LiNi_{0.5}Mn_{0.5}O_2$, $LiCoO_2$, and $LiNiO_2$. The solid line indicates the estimate for the lattice contribution to the heat capacity that was used to extract the magnetic contribution to overall heat capacity for $LiNi_{0.5}Mn_{0.5}O_2$.

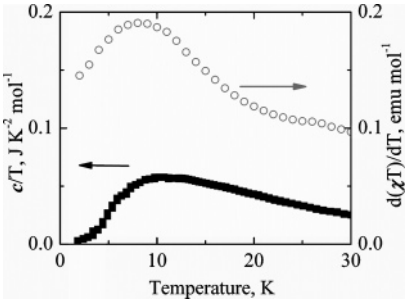

Figure 9. Magnetic specific heat of $LiNi_{0.5}Mn_{0.5}O_2$ derived from heat capacity and ac magnetic susceptibility measurements.

tures, as indicated by solid line in Figure 8. The magnetic contribution to the heat capacity obtained by subtraction of the lattice contribution shows a broad maximum centered at 10 K (Figure 9). A similar result is obtained by deriving an estimate of the magnetic heat capacity from $d(\chi T)/dT$[43] from the $\chi'(T)$ dependence ($f = 0.05$ Hz) (Figure 9). The wide maximum in the temperature dependence of the heat capacity is typical of glassy transitions;[40] therefore, the 10 K feature observed in the heat capacity data and the peaks observed in $\chi'(T)$ and $\chi''(T)$ at 13 and 7 K, respectively, may be attributed to the freezing of cluster magnetic moments. The large temperature difference between the $\chi'(T)$ and $\chi''(T)$ maxima indicates very slow spin relaxation times, which is consistent with the cluster glass freezing.

Magnetic Models. On the basis of the experimental results, it is now possible to estimate the sign and strength of the magnetic exchange between the transition metal ions, propose models for magnetic cluster formation, and compare them to the structural models of the compounds. The negative Curie−Weiss temperatures indicate that antiferromagnetic (AF) exchange dominates in these compounds. The strongest AF exchange is the 180° superexchange between interslab and TM layer Ni^{2+} ions. However, with increasing Co content, the amount of Ni^{2+} ions in the interslabs decreases by almost an order of magnitude to about 1% in the 333 compound, but the absolute Θ value decreases by less than half and the sign remains negative, indicating that in addition to the 180° AF superexchange, the strongest 90° exchange between ions within the TM layers is also antiferromagnetic.

In the TM layer, the MO_6 (M = Mn or Ni) octahedra share edges and the magnetic exchange may be either direct, mostly through t_{2g} orbitals, or mediated by oxygen orbitals. Following Goodenough's classification, two main superexchange mechanisms need to be considered. The first one is the delocalization mechanism, which assumes an electron drift from one cation to another. Generally, for the TM ions, $t_{2g}-t_{2g}$, e_g-t_{2g}, and e_g-e_g delocalization pathways are possible, but the strongest one for the case of edge-sharing octahedra is $t_{2g}-t_{2g}$ delocalization, because the t_{2g} orbitals spread toward each other, enabling direct exchange. For d^3-d^3 ($Mn^{4+}-Mn^{4+}$) magnetic exchange, this mechanism results in an AF interaction between half-filled t_{2g} orbitals; d^8-d^3 ($Ni^{2+}-Mn^{4+}$) transfer from a full (Ni^{2+}) to a half-filled (Mn^{4+}) t_{2g} orbital favors ferromagnetic (FM) exchange. In the d^8-d^8 ($Ni^{2+}-Ni^{2+}$) case, electron transfer between t_{2g} orbitals is not possible, $t_{2g}-e_g$ delocalization is very weak FM, and therefore e_g-e_g delocalization, which is AF, dominates. The second mechanism, called correlation, accounts for the simultaneous partial bond formation on each side of the anion. It can be realized in three different ways. First, anion s orbitals can form bonds with cation e_g orbitals. This exchange pathway is weak, since the O 2s orbitals lie at much lower energies than the metal 3d orbitals, and will not be considered here. Another correlation pathway is mediated by two O 2p electrons from the same p orbital, forming a σ-bond with an e_g orbital of one cation and π-bond with a t_{2g} orbital of the other cation. The third correlation possibility involves the simultaneous transfer of two electrons with the same-spin from two different oxygen 2p orbitals to e_g or t_{2g} orbitals of two TM cations. The last two pathways are efficient and consistent with each other, both predicting FM $Mn^{4+}-Mn^{4+}$ and AF $Mn^{4+}-Ni^{2+}$ interactions. In the case of $Ni^{2+}-Ni^{2+}$ correlation superexchange, only the third pathway is possible, giving FM exchange.

The delocalization and correlation mechanisms involving two Mn^{4+} t_{2g} orbitals predict opposite signs for this pairwise magnetic interaction. Both Goodenough[44] and Kanamori[45] attempted to resolve this problem and ended up with opposite

(43) Fisher, M. E. *Philos. Mag.* **1962**, *7*, 1731.
(44) Goodenough, J. B. *Magnetism and the Chemical Bond*; Interscience: New York, 1963.
(45) Kanamori, J. *J. Phys. Chem. Solids* **1959**, *10*, 87.

Table 2. Magnetic Exchange Pathways in $Li_xNi_{0.5}Mn_{0.5}O_2$

180°			90°		
$Ni^{2+}-Ni^{2+}$	$Ni^{2+}-Mn^{4+}$	$Ni^{3+}-Ni^{2+}$	$Ni^{2+}-Mn^{4+}$	$Mn^{4+}-Mn^{4+}$	$Ni^{2+}-Ni^{2+}$
AF very strong	FM strong	AF moderate	AF strong	FM moderate	FM weak

results; thus, experimental data for structurally related compounds are required to estimate the character and the strength of exchange interactions. For example, neutron diffraction studies of Li_2MnO_3, a compound built of alternating lithium layers and layers of Li^+ ions surrounded by six Mn^{4+} ions (as in the flower pattern), forming a so-called honeycomb arrangement of cations, show FM order of the Mn^{4+} spins within the honeycomb layers. The interlayer exchange in this material is antiferromagnetic and the compound undergoes an AF ordering transition at 36.5 K.[46] From this example, we can conclude that FM exchange of moderate strength is likely to be found between Mn ions in the 550 compound. The results also suggest that correlation superexchange is the dominant magnetic exchange mechanism within the TM layer; therefore, 90° Ni−Ni exchange should be FM and the Ni−Mn exchange AF. According to the Θ values, the latter interaction is the strongest. The signs and relative strengths of magnetic exchange pathways discussed are summarized in Table 2.

On the basis of the above magnetic interactions, ferrimagnetic order in the TM layers is predicted at low temperatures. In the case of the ideal layered structure, i.e., without any Ni in the lithium layer, AF exchange between the transition metal layers is predicted, on the basis of both the Goodenough rules extended to the M−O−Li−O−M pathway and from the Li_2MnO_3 example. Therefore, the magnetic moments of the TM layers should cancel and an AF ordering transition should be observed (Figure 10a). Our preliminary results for $NaNi_{0.5}Mn_{0.5}O_2$,[47] where Na/Ni exchange is not likely, confirm this hypothesis: an AF ordering transition is found at 55 K.

The magnetic properties of $LiNi_{0.5}Mn_{0.5}O_2$ are very different from those predicted above. We will now show that the presence of Ni in the Li layer dramatically changes the magnetic interactions and prevents AF ordering between the TM layers. When Ni ions are substituted into the Li layer, they participate in a 180° superexchange mechanism, with cations in the second cation coordination shell, mediated by the same (2p) oxygen orbitals responsible for the 90° correlation superexchange with cations in the first cation coordination shell. The 180° magnetic interactions are always stronger than the 90° interactions; therefore, the Ni^{2+} spins in the TM layer participating in 180° exchange should be aligned antiferromagnetically with respect to the Ni^{2+} ions in the Li layer. As a result, assuming the ideal flower structure (Figure 10b), four Ni^{2+} spins in the TM layers (per Ni in the Li layer) at the "corner" sites of the flower structure are aligned ferromagnetically. In practice, in the disordered structure proposed from the PDF analysis,[24] the number of ferromagnetically coupled Ni ions may be less. Ni ions in the lithium layer can also interact with the six cations in the first cation coordination shell. In the ideal flower structure, the interslab Ni^{2+} is nearby two Ni^{2+} and four Mn^{4+} ions (Figure 10b), resulting in Ni−Ni FM and Ni−Mn AF interlayer 90° interactions, respectively. These six ions are also coupled to the Ni^{2+} ions at the "corners" of the flower structure, leading to frustration. This frustration may impede ferrimagnetic ordering within TM layers.

The question as to whether the Mn^{4+} spins undergo magnetic ordering in this compound may be answered by using the EPR data available in papers by Stoyanova et al.[32,33] These data indicate that Mn^{4+} ions remain paramagnetic down to at least 60 K; however, below 60 K a broadening of EPR spectra is observed, and very broad spectra are found below 22 K. This allows us to conclude that the 96 K magnetic transition is caused solely by the ordering of Ni^{2+} spins involved in the 180° superexchange with interslab Ni^{2+} spins. In the case of the ideal stacking of the layers, i.e., providing a maximum number of 180° Ni−O−Ni bonds (Figure 1c), the magnetic clusters would propagate along the *c* direction and overall ferrimagnetic order involving Ni^{2+} spins in the corners of 12 Ni "flower" and those in the Li layer would be established. The disorder in the TM layer leads to the existence of some 180° Ni−O−Mn bonds with FM exchange of moderate strength and additional Ni−O−Li bonds breaking magnetic cluster propagation. Therefore, the 180° $Ni^{2+}-Ni^{2+}$ magnetic order is established within finite size clusters at 96 K. We note that our analysis differs from that of Abdel-Ghany et al., who assumed that the weaker 180° Ni−Mn interslab interactions were responsible for the onset of long-range ordering in $LiNi_{0.5}Mn_{0.5}O_2$.[34]

A transition from superparamagnetic to ferrimagnetic behavior was found in the $Li_xNi_{1-x}O$ compounds for $x < x_c = 0.432$, i.e., with increasing amount of Ni^{2+} in the lithium layer.[48] In $LiNiO_2$ and in the related compounds $LiNi_yTi_{1-y}O_2$ and $LiNi_{1-y}Al_yO_2$, the formation of magnetic clusters via the 180° exchange mechanism represents the sole reason for the low-temperature magnetization increase and magnetic hysteresis, as the intralayer magnetic exchange between Ni^{3+} ions is believed to be negligible.[46,49,50] The situation in $LiNi_{0.5}Mn_{0.5}O_2$ may be quite different, due to relatively strong 90° $Ni^{2+}-Mn^{4+}$ intralayer exchange. According to the $\chi''(T)$ and ZFC data, 180° Ni−Ni spin ordering is complete at about 60 K; however, the magnetization keeps increasing on lowering the temperature down to 20 K (Figure 2a), and a wide χ''(T) peak is observed between 60 and 20 K (Figure 5b). Magnetic ordering transitions in two structurally related compounds are observed in this temperature range. $NaNi_{0.5}Mn_{0.5}O_2$ orders AF at 55 K, which involves AF Ni−Mn 90° ordering, and Li_2MnO_3 undergoes AF ordering at 36.5 K, which involves FM Mn−Mn 90° ordering. Both compounds exhibit AF interlayer ordering. Therefore, an intralayer ordering of Mn^{4+} and Ni^{2+} spins may occur in this temperature region. Furthermore, a tiny shift of the whole $\chi'(T)$

(46) Strobel, P.; Lambert-Andron, B. *J. Solid State Chem.* **1988**, *75*, 90.
(47) Chernova, N. A.; Ma, M.; Xiao, J.; Whittingham, M. S.; Cabana, J.; Grey C. P. *Mater. Res. Soc. Symp. Proc.* **2007**, *972*, AA06−10.
(48) Mertz, D.; Ksari, Y.; Celestini, F. ; Debierre, J. M.; Stepanov, A.; Delmas, C. *Phys. Rev. B* **2000**, *61*, 1240.
(49) Croguennec, L.; Suard, E.; Willmann, P.; Delmas, C. *Chem. Mater.* **2002**, *14*, 2149.
(50) Guilmard, M.; Rougier, A.; Grune, M.; Croguennec, L.; Delmas, C. *J. Power. Sources* **2003**, *115*, 305.

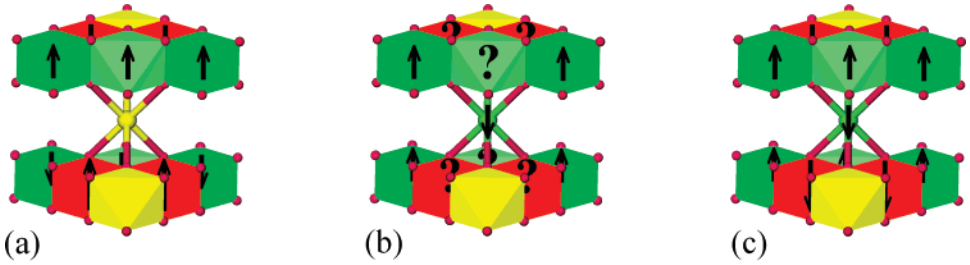

Figure 10. (a) Proposed AF spin alignment in $LiNi_{0.5}Mn_{0.5}O_2$ for the case of an ideal lithium layer containing no Ni^{2+} ions. The LiO_6 octahedra in the TM layer and lithium ion in the Li layer, yellow; MnO_6 octahedra, red; NiO_6, green. (b) Ferromagnetic spin alignment of Ni ions sharing corners with Ni in the Li layer (bright green); the frustrated Ni and Mn ions that share edges with the interslab Ni are indicated with question marks. (c) Ferrimagnetic ordering in the vicinity of Ni in the lithium layer.

and $\chi''(T)$ curves at 36.5 K (Figure 5) may reflect magnetic ordering in the Li-rich parts of the TM layer built of $LiMn_6$ clusters just like in Li_2MnO_3. The EPR studies by Stoyanova et al.[33] are consistent with this assumption, showing line broadening below 60 K and line shape change at 22 K.

Hinuma et al. observed overall FM Mn^{4+} spin ordering in their first-principle calculations, when using the GGA approximation, and FM intralayer with AF interlayer ordering in the GGA+U approximation.[35] The latter ordering scheme does not lead to a net magnetization increase, which contradicts our experimental observations. Therefore, FM ordering of the Mn^{4+} spins should occur, satisfying the AF Ni−Mn interactions within the TM layers (Figure 10c). Should this ordering occur in the perfect flower structure, this would result in a net magnetization of 0.83 μ_B per formula unit, assuming that Ni^{2+} spins in the "middle" sites are coupled FM to Ni^{2+} spins at the "corner" sites. In these calculations, saturation magnetizations of 3 μ_B per Mn^{4+} and 2 μ_B per Ni^{2+} ions were used. The experimental value of the net magnetization estimated as remanent magnetization at 5 K is about 0.13 μ_B per formula unit.

A mechanism that explains the low experimental value of the net magnetization may be proposed by considering a nonuniform distribution of Ni^{2+} in the lithium layer.[35] In the regions of higher Ni^{2+} content in the lithium layer, FM interlayer exchange is established as explained above; these regions contribute to the net magnetization and magnetization hysteresis. The local regions with no Ni^{2+} in the lithium layer may undergo AF intralayer ordering as in $NaNi_{0.5}Mn_{0.5}O_2$ and Li_2MnO_3 and, thus, do not contribute to the net magnetization. In both regions, Mn^{4+} spins contribute to the magnetic cluster formation within the TM layers, being AF coupled to Ni^{2+} spins and FM coupled to each other at low T (presumably, below 20 K). Thus, overall ferrimagnetic ordering within the layers is prevented due to the presence of Ni^{2+} in the lithium layer, and magnetic clusters of significant size are formed instead. The participation of Mn^{4+} spins in the magnetic cluster formation leads to a significant increase of magnetic cluster size, which is necessary to explain the large magnetization hysteresis. The freezing of the cluster magnetic moments occurs around 10 K, as indicated by the heat capacity and ac susceptibility data.

In the Co-containing compounds 442 and 333, the amount of Ni^{2+} in the TM layer progressively decreases to 0.045 and 0.01, respectively. In the presence of a significant amount of nonmagnetic Co^{3+} ions, the probability of magnetic cluster formation around those Ni^{2+} ions is smaller. The TM layers are magnetically separated and the AF exchange dominates within the layers, as follows from the negative Θ values. It is interesting to note that with two FM (Ni−Ni and Mn−Mn) and one AF (Ni−Mn) intralayer interaction there is no geometrical frustration between the nearest neighbors. The frustration required for the spin-glass state then comes from either next-neighbor or interlayer interactions. The other required condition for the spin-glass state is randomness, so no long-range TM order must be present in these compounds. No evidence for TM order was reported in 442; however, local TM ordering was observed in 333 compound by NMR, superlattice ordering was observed in the electron diffraction studies, and the ordered structure was found to have a negative formation energy.[51−53] Thus, an ordered structure may in principle exist to some extent, its coherence length in some of these compounds being large enough to observe superlattice ordering in electron diffraction, but a long-range magnetic ordering is not achieved as some disorder, both intralayer and stacking, drives the system into a spin-glass state.

Magnetic and Structural Changes upon Li Cycling in $LiNi_{0.5}Mn_{0.5}O_2$. We have studied the evolution of the magnetic properties of the 550 compound upon electrochemical charge and discharge, in order to understand the structural changes, particularly the proposed transition metal ion migrations and oxidation/reduction processes, through the magnetic properties. This work complements neutron and X-ray diffraction, ^{6}Li MAS NMR studies, and the first-principle calculations efforts directed toward understanding of cycling behavior of this compound.[39]

The temperature dependences of the magnetic susceptibilities and their reciprocals corrected due to presence of the Teflon binder and/or graphite in the samples are presented in Figure 11. Upon decrease of the lithium content during charging, the slope of the high-temperature Curie−Weiss parts of the reciprocal susceptibilities increases, indicating a decrease of the magnetic moment as Ni^{2+} ($S = 1$) is oxidized to Ni^{3+} ($S = {}^1/_2$) and then to low-spin Ni^{4+} ($S = 0$). The decrease of the Curie−Weiss temperatures indicates that the magnetic exchange between the transition metal ions weakens. The increase of susceptibility ascribed to the partial

(51) Cahill, L. S.; Yin, S. C.; Heinmaa, I.; Nazar, L. F.; Goward, G. R. *Chem. Mater.* **2005**, *17*, 6560.
(52) Koyama, Y.; Tanaka, I.; Adachi, A.; Makimura, Y.; Ohzuku, T. *J. Power Sources* **2003**, *119-121*, 644.
(53) Yabuuchi, N.; Koyama, Y.; Nakayama, N.; Ohzuku, T. *J. Electrochem. Soc.* **2005**, *152*, A1434.

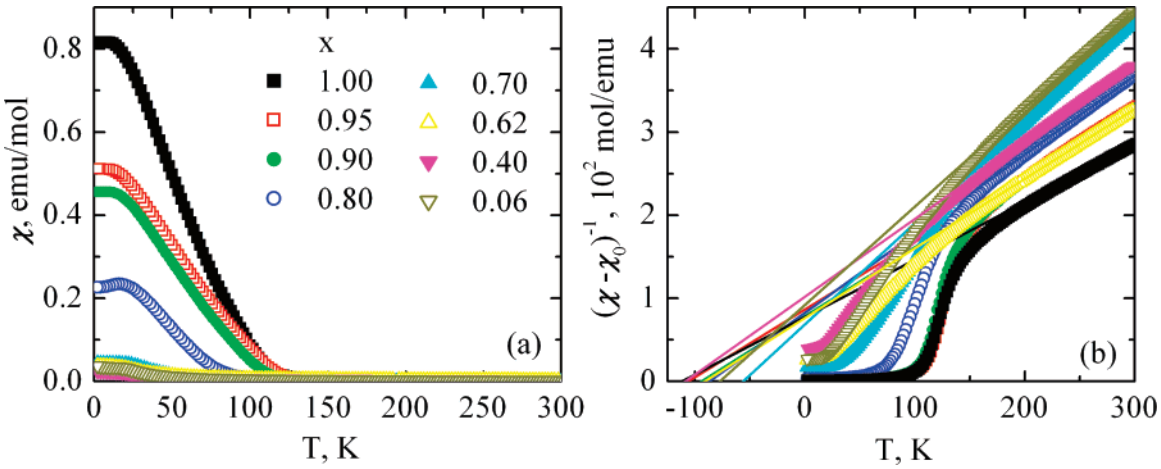

Figure 11. (a) Temperature dependences of magnetic susceptibilities of electrochemically delithiated $Li_xNi_{0.5}Mn_{0.5}O_2$. (b) The reciprocal susceptibilities and their fit to the Curie−Weiss law.

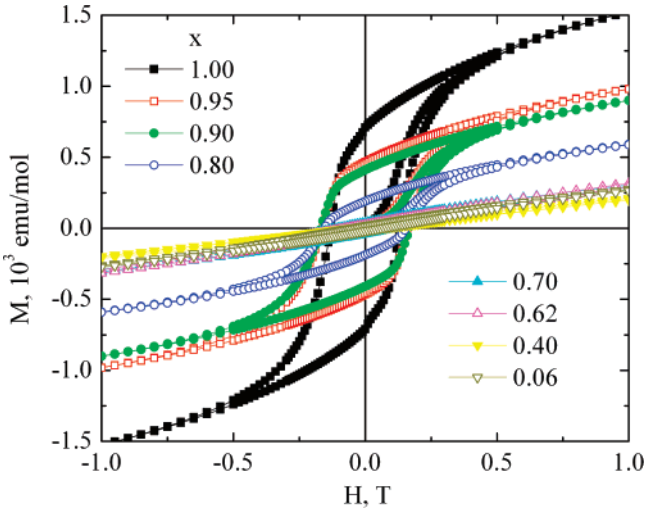

Figure 12. Magnetization curves of electrochemically delithiated $Li_xNi_{0.5}Mn_{0.5}O_2$.

ferrimagnetic cluster ordering reaches saturation at lower values of the susceptibility, and the magnetic ordering transition temperature shifts toward lower temperatures with lithium removal. The changes seen in the early stages of charge (i.e., for $x = 0.95$, 0.9 and 0.8) can be ascribed solely to the oxidation of Ni^{2+} ions, but for $x \leq 0.7$, the shape of the $\chi(T)$ dependence becomes similar to that of the 442 and 333 Co-containing samples, indicating significant changes in the magnetic interactions. The same trend is found in the magnetization curves (Figure 12). At the beginning of charge the hysteresis loop decreases in size, but preserves its shape, while for $x \leq 0.7$ a flat hysteresis loop similar to that of the 442 compound is observed.

The magnetic parameters for the two sets of samples are summarized in Table 3 and presented in Figure 13. These data follow the above trends in the two sets of samples; however, there is little consistency between the two sets of data. For example, samples charged in the large cell show better agreements between the experimental and theoretical magnetic moments per TM ion, calculated by assuming a progressive oxidation of Ni^{2+} to Ni^{3+} to (low-spin, $S = 0$) Ni^{4+}, while the experimental μ values of the samples charged in small cells are always lower than the theoretical ones, the difference increasing with the degree of charge. The

Table 3. Magnetic Parameters of the Electrochemically Delithiated $Li_xNi_{0.5}Mn_{0.5}O_2$ Compounds

x	voltage	C, emu K/mol	Θ, K	μ_{exp}, μ_B	μ_{theor}, μ_B	M_r, emu/mol	H_c, Oe
			Small Cells				
1.00		1.446(4)	−111.8(6)	3.40(1)	3.39	710.0	1316(2)
0.95		1.228(2)	−106.1(3)	3.13(1)	3.35	466.9	1640(2)
0.90		1.204(1)	−94.4(2)	3.10(1)	3.32	410.0	1681(2)
0.80		1.051(2)	−86.8(3)	2.90(1)	3.24	189.9	1556(1)
0.70		0.820(1)	−56.1(2)	2.56(1)	3.16	38.6	1077(1)
0.40	4.8	0.791(1)	−73.3(2)	2.52(1)	2.95	21.3	1055(5)
0.06	5.3	0.689(1)	−50.0(2)	2.35(1)	2.77	25.4	1114(20)
			Large Cells				
0.62	4.1	1.193(4)	−91.0(6)	3.08(1)	3.10	25.1	751(2)
0.40	4.8	1.068(2)	−108.9(3)	2.92(1)	2.95	14.7	633(1)
0.06	5.2	0.843(2)	−77.4(4)	2.60(1)	2.77	18.9	576(1)
			Samples after One Cycle				
0.9	4.5−2	1.228(2)	−124.7(4)	3.13(1)	3.32	342.8	1800(8)
0.9	4.6−2	1.398(1)	−143.5(1)	3.34(1)	3.32	339.9	1559(1)
0.86	4.8−2	1.363(4)	−120.0(4)	3.29(1)	3.29	307.2	1467(2)
0.73	5.3−2	1.245(3)	−96.6(4)	3.13(1)	3.19	306.1	1442(1)

[a] Theoretical magnetic moments are calculated by assuming oxidation of Ni^{2+} ($S = 1$) to Ni^{3+} ($S = 1/2$) and then to Ni^{4+} ($S = 0$) upon lithium removal.

reasons for such a discrepancy may be that the large cells were better equilibrated, were free of binder, and that they provided more material for the magnetic studies, ensuring more accurate determination of the magnetic moment and other parameters. These data show *no* evidence for the formation of high-spin Ni^{4+}, as suggested in the previous magnetic study,[34] since in this case, the μ_{exp} is expected to be larger than μ_{theor}.

The dependences of the coercivity and remanent magnetization upon Li content (Figure 13c,d) clearly indicate a change of magnetic behavior at $x \approx 0.7$. Above this value, both parameters increase as the lithium content increases, while below $x \approx 0.7$ they show saturation. The coercivity values remain significant, around 500−1000 Oe, even at the top of charge, while the remanence drops by more than 1 order of magnitude. The latter indicates that at some point of charge, which we believe is $x \approx 0.7$, the magnetic clusters are destroyed. According to the neutron diffraction data,[39] no significant change of Ni content in the lithium layer is observed at this state of charge. This occurs later, at between 4.6 and 4.8 V, at a lithium content of around 0.4. Therefore, the magnetic cluster destruction should only be caused by

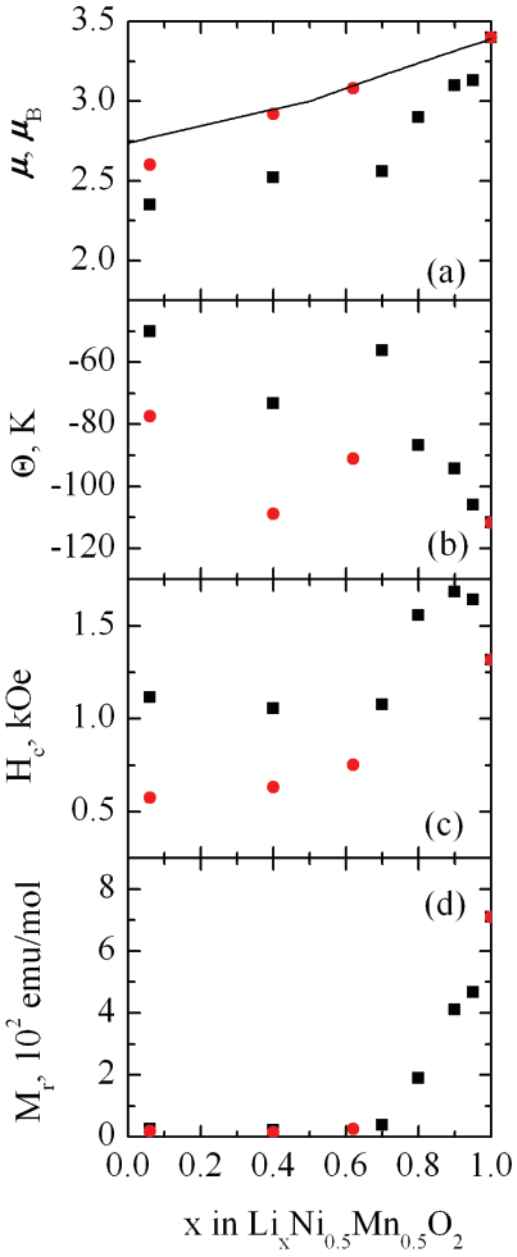

Figure 13. Dependences of (a) the average effective magnetic moment per TM ion, the solid line representing the theoretical dependence assuming consecutive oxidation of Ni^{2+} ($S = 1$) to Ni^{3+} ($S = 1/2$) to Ni^{4+} ($S = 0$), (b) Curie−Weiss temperature, (c) coercivity, and (d) remanence, on the lithium content x in $Li_xNi_{0.5}Mn_{0.5}O_2$. Data for samples charged in small cells are plotted as squares and in large cells as circles.

the decrease in magnetic exchange due to oxidation of Ni^{2+} to Ni^{4+}, via Ni^{3+}.

The extremely rapid decrease of magnetization observed at the beginning of charge suggests that either the Ni^{2+} ions from the TM layer participating in 180° superexchange (i.e., the "corner" Ni ions in the ideal flower structure) or the interslab Ni ions are oxidized first. Oxidation of interslab Ni^{2+} ions is not consistent with the increase in the c-parameter seen during the early stages of charge and theoretical calculations for this system.[39] Furthermore, no evidence for the oxidation of the interslab ions was seen in earlier data for disordered $LiNiO_2$ samples. Thus, the data suggest that the "corner" Ni ions of the flower structure are largely oxidized first (i.e., for $x = 1$ to approximately 0.7),

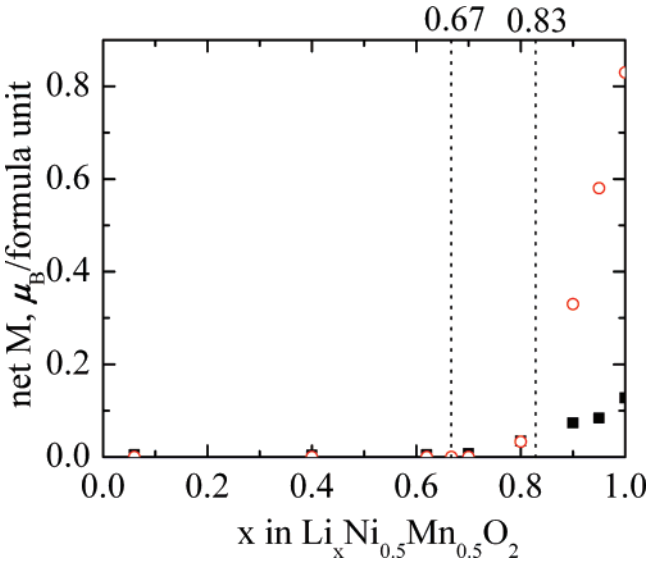

Figure 14. Net magnetization as a function of lithium content x in $Li_xNi_{0.5}Mn_{0.5}O_2$. Squares represent experimental remanent magnetizations, and circles represent the theoretical values obtained from the model described in the text.

before the "middle" ions, on charging $Li_xNi_{0.5}Mn_{0.5}O_2$. The decrease of magnetization is then ascribed to weaker magnetic exchange involving Ni^{3+} ions or the formation of diamagnetic Ni^{4+} ions, even at low states of charge. An octahedrally coordinated Ni^{3+} ion with a $t_{2g}^6e_g^1$ electronic configuration is subject to a Jahn−Teller distortion, lifting the degeneracy of the e_g orbitals. Even a dynamic Jahn−Teller effect may significantly weaken the 180° Ni^{2+}−Ni^{3+} and 90° Mn^{4+}−Ni^{3+} and Ni^{2+}−Ni^{3+} exchange pathways destroying the magnetic clusters. The existence of magnetic clusters in $LiNiO_2$ indicates that the 180° Ni^{2+}−Ni^{3+} exchange is likely to remain relatively strong.[48] By contrast, if the ferrimagnetic ordering of Ni and Mn spins within the TM layers was preserved upon oxidation of Ni^{2+} to Ni^{3+}, it would result in an increase of the magnetic moment as the smaller magnetic moment of Ni^{3+} would reduce the cancellation of the Ni and Mn^{4+} magnetic moments in the TM layers. This is not consistent with the experimental data, indicating that 90° Mn−Ni and Ni−Ni magnetic exchange pathways are destroyed upon oxidation of Ni^{2+} to Ni^{3+}. The Mn−Mn FM order within the TM layers may still exist, but the weakening of Ni−Mn exchange allows AF order between the layers, which effectively reduces the net magnetization.

In the study of lithium deintercalation process by Arachi et al.,[54] a structural transition to a monoclinic phase was found at $x = 0.7$ from the synchrotron X-ray diffraction data. One of the possible reasons for this transition is the Jahn−Teller distortion. The transition was not found in the neutron diffraction data of our samples,[39] possibly due to lower resolution of the neutron diffraction data as compared to the synchrotron X-ray diffraction data; however, the weakening of the 180° magnetic exchange found at the same $x = 0.7$ value supports the occurrence of at least a local structural distortion.

(54) Arachi, Y.; Koabayashi, H.; Emura, S.; Nakata, Y.; Tanaka, M.; Asai, T.; Sakaebe, H.; Tatsumi, K.; Kageyama, H. *Solid State Ionics* **2005**, *176*, 895.

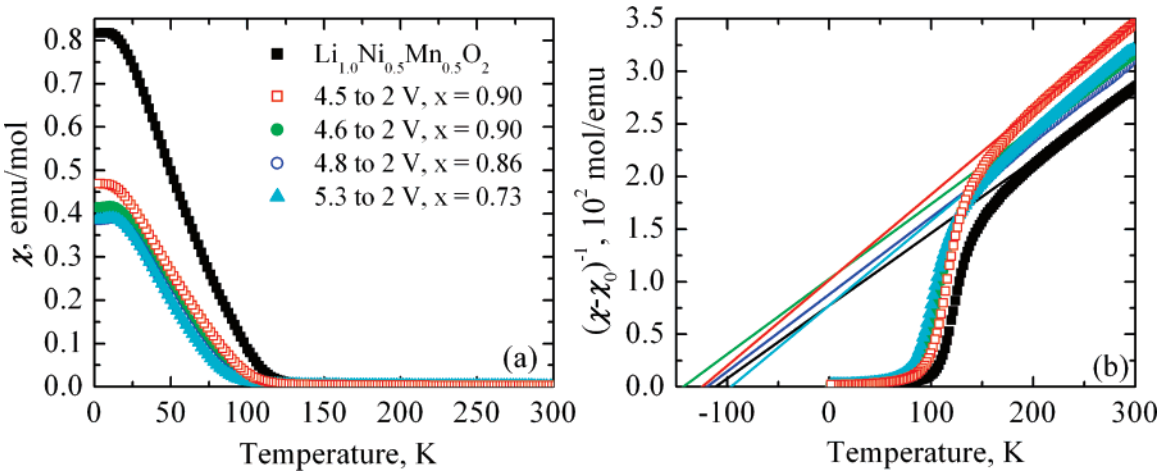

Figure 15. Temperature dependences of the magnetic susceptibilities of $Li_xNi_{0.5}Mn_{0.5}O_2$ after one cycle (a), and the reciprocal susceptibilities and their fits to the Curie−Weiss law (b). The pristine $LiNi_{0.5}Mn_{0.5}O_2$ data are shown for comparison.

Interestingly, the electrochemical profile observed on charging this material is very flat in the range $0.7 \leq x \leq 1$ and then starts to increase steadily for $x < 0.7$, suggesting that the mechanism is different before and after 0.7. The formula of the flower structure can be written as $Li_{11/12}$-$Ni_{1/12}[Li_{1/12}Ni(corner)_{2/12}Ni(middle)_{3/12}Mn_{6/12}]O_2$, and assuming that the 0.167 per formula unit corner Ni^{2+} ions are oxidized first to Ni^{4+}, this will be associated with the removal of approximately 0.333 Li per formula unit, consistent with the electrochemical profile and the magnetic properties. Van der Ven and Ceder suggested[26] that the initial process, at least in the ideal flower structure, involved the removal of Li from the TM layer (one per flower unit), the formation of two tetrahedral sites per Li in the TM layer (two per flower unit), and the removal of four Li (per flower unit) in the Li layer; i.e., three Li are removed out of a total of 12/flower unit (0.25 Li per formula unit). This process is associated with the oxidation of 0.25 Ni^{2+} ions to Ni^{3+} or 0.125 Ni^{2+} to Ni^{4+}. Our results are not inconsistent with this prediction and further suggest that the oxidation of the "corner" Ni ions is associated with the removal of Li from the TM layer. Clearly, if we oxidize these Ni^{2+} initially, then the stabilization energy associated with the Ni−O−Ni superexchange is lost. However, on the basis of simple Coulombic arguments, we would expect the corner sites to be oxidized first, since they are closer to fewer Mn^{4+} ions (corner and middle sites are nearby three and four Mn^{4+} ions, respectively) and are more distant from the interslab Ni^{2+} ions, reducing the unfavorable $Ni^{3+}/Ni^{4+}-Mn^{4+}$ and $Ni^{3+}/Ni^{4+}-Ni^{2+}$ Coulombic interactions.

We have estimated the magnitude of the net magnetization as a function of lithium content x in $Li_xNi_{0.5}Mn_{0.5}O_2$ assuming the ideal flower structure with magnetic order presented in Figure 10c for $x = 1$. We assume that upon Li removal ($0.83 \leq x < 1$) Ni ions in the "corner" sites are first oxidized to Ni^{3+}. Each "corner" Ni^{3+} has 3 Mn^{4+} and 1.5 Ni^{2+}(middle) nearest neighbors per formula unit, which are considered "paramagnetic" according to our earlier suggestion that 90° superexchange pathways involving Ni^{3+} ions are very weak. Thus, at $x = 0.83$ only 180°-bound $Ni^{2+}-Ni^{3+}$ clusters exist, which, ideally, should have a zero magnetic moment as the ratio of Ni^{2+} in the Li layer to "corner" Ni^{3+} is 1:2. In the disordered structure, a net magnetic moment should, however, be observed. If further oxidation ($0.67 \leq x < 0.83$) occurs at "middle" Ni sites, no change to the net magnetization should be observed, as the "middle" Ni ions are already considered "paramagnetic". The oxidation of "corner" Ni^{3+} to Ni^{4+} would result in a magnetization decrease due to destruction of magnetic clusters. The calculated net magnetizations obtained on the basis of this analysis are presented in Figure 14 together with experimental remanent magnetization values. In the $0.83 \leq x < 1$ region, the experimental magnetization is much lower than the calculated one, which is consistent with the existence of AF ordered regions, as suggested earlier. An additional reason for this discrepancy may be a particle size and shape effect not accounted for in the estimation of experimental magnetization values. Due to both of these factors, the amount of Ni in the Li layer cannot be readily determined from the magnetic characteristics by a simple division of the observed magnetization by the estimated magnetic moment of one magnetic cluster, as was performed in ref 34. The experimentally determined relative drop of magnetization upon lithium removal is, however, fairly close to the calculated value. For example, upon removal of 0.05 Li, the remanent magnetization decreases by 35%, while the calculated value decreases by 30%. In the $0.67 \leq x < 0.83$ region the experimental magnetization values agree reasonably well with those obtained by assuming that only 180° ferrimagnetic $Ni^{2+}-Ni^{3+}$ cluster ordering exists in this region. Whether all the corner Ni ions are oxidized to Ni^{4+} so early on in the charge process is still not clear. Remanent magnetization in the $0.67 \leq x < 0.83$ region may exist due to either disorder or oxidation of corner Ni^{3+} ions to Ni^{4+}, making it difficult to use this method to quantify the Ni oxidation state on charge.

The magnetic data for the samples discharged to 2 V after being charged to different voltages is presented in Figures 15 and 16. All the samples show similar magnetic properties: a pronounced increase of susceptibility below 100 K and wide hysteresis loops. The magnetic moments calculated from the reciprocal susceptibilities are consistent with Ni reduction back to Ni^{2+} upon Li intercalation (Table 2). Hence, one can conclude that upon reduction of Ni back to 2+ the magnetic clusters around the Ni^{2+} ions in the Li layer

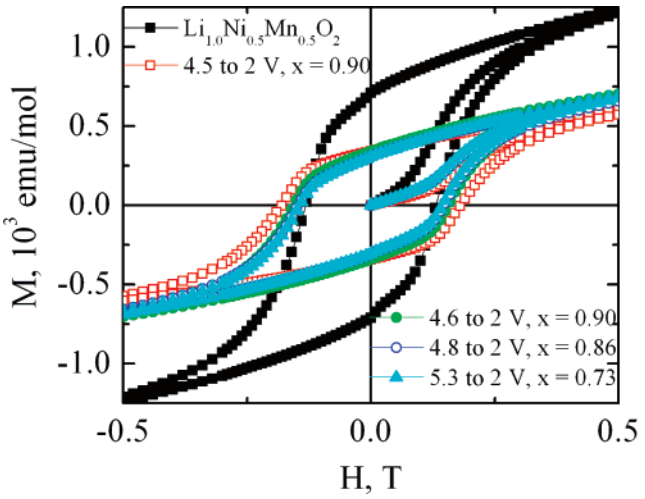

Figure 16. Magnetization curves of $Li_xNi_{0.5}Mn_{0.5}O_2$ after one cycle; the pristine $LiNi_{0.5}Mn_{0.5}O_2$ data are shown for comparison.

are restored and include 180° $Ni^{2+}-Ni^{2+}$ and 90° $Ni^{2+}-Mn^{4+}$ spin ordering as in the pristine compound. This data is consistent with the neutron diffraction data showing that upon discharge most (60%) of the Ni ions that migrated to the TM layer at high voltages return to the lithium layer.[39] The smaller values of H_c and M_r observed on discharge are then ascribed to the reduced Ni content in the Li layer and/or some residual Ni^{3+} ions in the sample. Furthermore, according to the neutron diffraction data, the sample discharged from 5.2 V contains about 0.038 Ni ions/formula unit in the tetrahedral sites. Clearly, these ions do not destroy the magnetic clusters. Possibly, the tetrahedral Ni ions can contribute to the magnetic cluster formation in addition to the octahedral Ni in the Li site. This is not unreasonable, since the Ni−O−Ni angle in this case is about 125°, and the 180° superexchange mechanism is still valid; for example, strong AF interactions between tetrahedral and octahedral sites occur in the spinel structure.

$LiNi_{0.5}Mn_{0.5}O_2$ charged to potentials above 4.6 V is typically associated with an irreversible capacity of as much as 50 mA h g^{-1}.[39] In the Li-excess materials $Li[Ni_xMn_{(2-x)/3}Li_{(1-2x)/3}]O_2$, at least some of this irreversible capacity seen in these systems is ascribed to oxygen loss at high voltages,[55] a process that should be accompanied by the reduction of Ni^{4+} to Ni^{3+}, limiting the capacity of the material on discharge. The magnetic susceptibility measured here for $LiNi_{0.5}Mn_{0.5}O_2$ shows that residual Ni^{3+} ions are left in the sample on discharge, indicating that on discharge there are parts of the sample that cannot be readily reduced to Ni^{2+} at least in this voltage window.

Conclusion

The magnetic properties of $LiNi_{0.5}Mn_{0.5}O_2$ are explained by assuming an imperfect "flower" ordering of the transition metal ions in the transition metal layers. At low temperature, Mn spins and Ni spins in the TM layer are ordered antiferromagnetically, generating a net magnetic moment. The nonuniform distribution of Ni in the lithium layer causes AF interlayer exchange and net magnetic moment cancellation in Ni-poor regions of the Li layers and FM interlayer exchange mediated by strong 180° $Ni^{2+}(TM)-Ni^{2+}(Li)$ exchange in Ni-rich regions. No long-range magnetic order is established, which is confirmed by the heat capacity and neutron diffraction data; large magnetically ordered clusters are formed instead. These clusters are formed through a series of magnetic transitions. The magnetic transition at 96 K is attributed to the ordering of the Ni^{2+} spins from both TM and lithium layers coupled by strong 180° antiferromagnetic superexchange. The intralayer ordering of Mn and Ni spins occurs between 60 and 20 K. Cluster magnetic moments undergo a freezing transition at about 10 K, as evidenced by the heat capacity and ac susceptibility data. With increasing Co^{3+} content the amount of interslab Ni^{2+} ions decreases; Ni^{2+} ions coupled by 180° exchange form smaller clusters due to dilution with nonmagnetic Co^{3+} ions, which results in the cluster-glass behavior found in $LiNi_{0.45}Mn_{0.45}Co_{0.1}O_2$. A further increase in the Co content makes cluster formation even less probable due to significant dilution of the Ni/Mn lattice with nonmagnetic Co^{3+} ions. This results in the spin-glass transitions at 10 and 7 K found in $LiNi_{0.4}Mn_{0.4}Co_{0.2}O_2$ and $LiNi_{1/3}Mn_{1/3}Co_{1/3}O_2$, respectively.

Upon electrochemical delithiation, Ni^{2+} ions are oxidized to Ni^{3+} and then to Ni^{4+}. When approximately 0.3 Li is removed, the magnetic clusters formed around the Ni^{2+} ions in the Li layer are destroyed. As no change in the concentration of such Ni ions was found at this stage of charge in the neutron diffraction studies and the oxidation of these ions is not likely,[39] the destruction of magnetic clusters was explained by significantly weaker 90° magnetic exchange involving Ni^{3+} ions in the TM layer as a result of Ni^{3+} Jahn−Teller distortion. A Jahn−Teller distortion is consistent with Arachi's et al. observation of the structural transition when 0.3 lithium is removed.[54] Furthermore, the results suggest that the Ni^{2+} ions in the TM layer involved in the 180° magnetic exchange are preferentially oxidized before the remaining Ni^{2+} sites. Upon discharge, Ni ions are reduced back to Ni^{2+}; their content in the Li layer is partially restored,[39] and the magnetic order described above resumes.

Acknowledgment. We thank the US Department of Energy, Office of FreedomCAR and Vehicle Techologies, for financial support through the BATT program at Lawrence Berkeley National Laboratory. Financial support from the National Science Foundation, DMR 0705657, is greatly appreciated. James O'Brien from Quantum Design is acknowledged for the acquisition of the heat capacity data. We thank Thomas Proffen from Los Alamos National Laboratory for the help with the neutron diffraction experiments. This work has benefited from the use of NPDF at the Lujan Center at the Los Alamos Neutron Science Center, funded by the DOE Office of Basic Energy Sciences (BES), Los Alamos National Laboratory, and the DOE under Contract No. W-7405-ENG-36.

Supporting Information Available: Neutron diffraction patterns for $LiNi_{0.5}Mn_{0.5}O_2$ at 300, 120, and 60 K and the Rietveld refinement results (PDF). This material is available free of charge via the Internet at http://pubs.acs.org.

CM0708867

(55) Armstrong, A. R.; Holzapfel, M.; Novak, P.; Johnson, C. S.; Kang, S. H.; Thackeray, M. M.; Bruce, P. G. *J. Am. Chem. Soc.* **2006**, *128*, 8694.